# Effects of overlapping parametric resonances on the particle diffusion process

C. M. Chu,[1] M. Ball,[1] B. Brabson,[1] J. Budnick,[1] M. Ellison,[1] K. M. Fung,[1] B. Hamilton,[1] W. C. Hsi,[1] D. Jeon,[1] X. Kang,[1] L. L. Kiang,[1] S. Y. Lee,[1] K. Y. Ng,[2] A. Pei,[1] A. Riabko,[1] and T. Sloan[1]
[1]*Department of Physics, Indiana University, Bloomington, Indiana 47405*
[2]*Fermilab, Box 500, Batavia, Illinois 60510*
(Received 19 April 1999)

The evolution of the beam distribution in a double-rf system with a phase modulation on either the primary or secondary rf cavity was measured. We find that the particle diffusion process obeys the Einstein relation if the phase space becomes globally chaotic. When dominant parametric resonances still exist in the phase space, particles stream along the separatrices of the dominant resonance, and the beam width exhibits characteristic oscillatory structure. The particle-tracking simulations for the double-rf system are employed to reveal the essential diffusion mechanism. Coherent octupolar motion has been observed in the bunch beam excitation. The evolution of the longitudinal phase space in the octupole mode is displayed. [S1063-651X(99)00111-7]

PACS number(s): 29.27.Bd, 41.75.−i, 05.45.−a

## I. INTRODUCTION

In particle beam physics, controlled particle diffusion has many applications. This includes the uniformization of the phase-space painting for beam injection, controlled beam dilution for minimizing uncontrollable emittance growth due to collective instabilities, stochastic beam scraping, stochastic slow beam extraction, etc. In the past, a secondary high-frequency rf system was employed for attaining a controlled longitudinal beam emittance dilution, so that negative mass instability across the transition energy can be minimized [1,2]. The procedure was to modulate the phase of a secondary rf system for a controlled beam dilution before the transition energy crossing. Earlier theoretical studies indicated that the diffusion mechanism was dominated by a single parametric resonance [1]. However, a single parametric resonance can hardly lead to a desired uniform distribution in the longitudinal phase space [3]. In contrast, we find that the diffusion process is dominated by the chaos generated by overlapping resonances [4].

Sources of random noise such as the quantum fluctuation, rf noise, intrabeam scattering, etc., play an important role in beam physics. These random noise sources can usually be represented by the Langevin force in the equation of motion [5]. When particles are acted on by the Langevin force, they diffuse in phase space. Applying the central limit theorem for the random statistically independent noise, the mean-square width of the beam distribution at time $t$ satisfies the Einstein relation $\sigma^2 \approx \mathcal{D}t$, where $\mathcal{D}$ is the diffusion coefficient. However, there are many diffusion processes that do not obey the Einstein relation. One such diffusion process is usually called *anomalous diffusion* [6]. Examples of anomalous diffusion can be found in plasma physics, Lévy dynamics, turbulent flow, space-charge dominated beams [7], etc. The source and the mechanism of anomalous diffusion are of considerable interest in physics in recent years.

In the past few years, beam dynamics experiments at the Indiana University Cyclotron Facility (IUCF) Cooler Ring were devoted mainly to the study of single-particle effects in the presence of nonlinear resonances [8]. This paper reports results of recent beam physics experiments that explore the particle diffusion mechanism in the study of beam manipulation techniques.

The experiments at the IUCF Cooler Ring employed a primary rf system operating at the harmonic number $h_1=1$ and a secondary rf system at $h_2=9$. A secondary rf cavity operating at a higher harmonic number can flatten the rf potential well to reduce the peak current and increase the synchrotron tune spread for Landau damping [9]. The equilibrium beam profile, conforming with the shape of the potential well, allows a higher ratio of the average current to the peak current. Furthermore, the increase in the synchrotron tune spread provides higher threshold current for the collective instabilities. Such double-rf systems have been successfully applied to several low-energy storage rings and synchrotron light sources [9,10]. In our experiments, phase modulation was applied to one of the rf systems. We studied the particle diffusion mechanism in the longitudinal phase space, checked the Einstein relation, and examined the effects of overlapping parametric resonances.

This paper is organized as follows. In Sec. II, the synchrotron equation of motion for the double-rf system with rf phase modulation is formulated. The effect of noise and phase space damping with electron cooling will be discussed. In Sec. III, we discuss experimental setup and method. In Sec. IV, we present the results of our experiments and data analysis. The conclusion is given in Sec. V. Theoretical analysis is given in Appendix A.

## II. SYNCHROTRON EQUATION OF MOTION

Let $\phi=-h_1(\tilde{\theta}-\tilde{\theta}_s)$ and $\delta=(h_1|\eta|/\nu_s)(\Delta p/p_0)$ be the normalized conjugate phase-space coordinates, where $h_1$ is the harmonic number of the primary cavity, $\tilde{\theta}$ and $\tilde{\theta}_s$ are, respectively, the orbiting angles of nonsynchronous and synchronous particles, $\eta$ is the phase-slip factor, $p_0$ is the momentum of a synchronous particle, $\Delta p=p-p_0$ is the momentum deviation, $\nu_s=[h_1 e V_1|\eta|/(2\pi\beta^2 E)]^{1/2}$ is the synchrotron tune, $V_1$ is the voltage of the primary rf cavity, and $e$, $\beta$, and $E$ are the electric charge, the Lorentz velocity factor, and the energy of the particle. The synchrotron equa-

 

tion of motion for a particle in a single rf system is given by

$$\dot{\phi} = \nu_s \delta, \tag{1}$$

$$\dot{\delta} = -\nu_s \sin\phi, \tag{2}$$

where the overdot corresponds to the derivative with respect to ''time'' coordinate $\theta = \omega_0 t$, where $\omega_0 = 2\pi f_0$ is the angular revolution frequency of a synchronous particle. The equation of motion can be derived from an unperturbed Hamiltonian

$$H_0 = \frac{1}{2}\nu_s \delta^2 + \nu_s(1-\cos\phi). \tag{3}$$

In the presence of quantum fluctuation with white noise and beam cooling, the synchrotron motion can be modeled as

$$\dot{\delta} = -\nu_s \sin\phi - \lambda\delta + D\xi, \tag{4}$$

where $\lambda$ is the damping decrement, and the Gaussian white noise function $\xi$ satisfies

$$\langle \xi(\theta)\xi(\theta')\rangle = \delta(\theta-\theta'), \quad \langle\xi\rangle = 0,$$

where the angled brackets represent ensemble average and $D$ is the amplitude of the white noise that may arise from beam-gas scattering, intrabeam scattering, rf noise, and other noise sources in a storage ring. At a typical IUCF Cooler Ring operation condition, $\lambda$ and $D$ are approximately $3\times10^{-6}$ and $2\times10^{-4}$, respectively [8]. The equilibrium particle distribution function that satisfies the Fokker-Planck-Vlasov equation of the stochastic dynamical system with white noise is given by [5]

$$\rho(\phi,\delta) = \frac{1}{\mathcal{N}} e^{-H_0/E_0}, \tag{5}$$

where $\mathcal{N}$ is a normalization constant with $\int \rho(\phi,\delta)d\phi\, d\delta = 1$ and the ''thermal energy'' of the beam is

$$E_0 = D^2/2\lambda. \tag{6}$$

In the presence of a secondary rf system with phase modulation, the synchrotron equation of motion of Eq. (4) becomes

$$\dot{\delta} = -\nu_s[\sin(\phi+\Delta\phi_1) - r\sin(h\phi+\Delta\phi_2)] - \lambda\delta + D\xi, \tag{7}$$

where $r = V_2/V_1$ is the ratio of the voltage $V_2$ of the secondary rf cavity to the voltage $V_1$ of the primary rf cavity and $h = h_2/h_1$ is the ratio of their respective harmonic numbers. The sinusoidal phase-modulation terms $\Delta\phi_1$ and $\Delta\phi_2$ are

$$\Delta\phi_1 = A_1 \sin(\nu_{m1}\theta), \tag{8}$$

$$\Delta\phi_2 = A_2 \sin(\nu_{m2}\theta) + \Delta\phi_0, \tag{9}$$

where $A_1$ and $A_2$ are the modulation amplitudes, $\nu_{m1} = f_{m1}/f_0$ and $\nu_{m2} = f_{m2}/f_0$ are the modulation tune with modulation frequencies $f_{m1}$ and $f_{m2}$, $f_0$ is the revolution frequency of a synchronous particle, and $\Delta\phi_0$ is the relative phase differences between two rf systems. Without damping and the random noise terms, the modulation Hamiltonian for synchrotron motion is

$$H = \frac{1}{2}\nu_s\delta^2 + \nu_s\left\{1-\cos(\phi+\Delta\phi_1) + \frac{r}{h}[1-\cos(h\phi+\Delta\phi_2)]\right\}. \tag{10}$$

The objective of this paper is to study the dynamics of enhanced particle diffusion in the presence of phase modulation. Properties of the time-dependent Hamiltonian will be discussed in the Appendix.

## III. EXPERIMENTAL SETUP AT THE IUCF COOLER RING

The IUCF Cooler ring is a six-sided proton storage ring with electron cooling. Protons can be accelerated or stored from 45 to 500 MeV in kinetic energy. In the experiment, the beam currents were maintained between 100 to 500 $\mu$A for a single bunch in the ring at 45 MeV.

In the Cooler ring, there are two rf acceleration cavities; the primary MPI cavity operates at a harmonic number $h_1 = 1$ and the secondary PPA cavity operates at the harmonic number $h_2 = 9$. The choice of $h_2 = 9$ is limited by the frequency range of the PPA cavity. The results of our study do not depend on the choice of $h_2$ provided that $h_2 \gg h_1$ (see Sec. IV B 3).

In our experiment, a 90 MeV $H_2^+$ beam from the K200 cyclotron was strip-injected into the Cooler ring resulting in a 45 MeV kinetic energy proton beam. The revolution frequency was $f_0 = 1.031\,680$ MHz and only the primary rf system with $h_1 = 1$ was active before our data taking. After injection, the proton beam was cooled by the electron cooling system to reduce the beam emittances. The electron cooling rate at the Cooler ring was measured to be about $3 \pm 1\ \mathrm{s}^{-1}$ at this energy [8]. The accelerator cycle time was set at 10 s, and the secondary rf system and the data acquisition system were turned on at 3 s after the completion of injection, i.e., the beam had been cooled to a stationary state in the primary rf system. The rms bunch length of the cooled beam was about 15–20 ns with an rms fractional momentum spread about $8\times10^{-5}$. The primary rf voltage was set at about 300 V, which, by itself, resulted in a synchrotron frequency $f_{syn}$ of about 705 Hz.

The beam profile was taken from a BPM sum signal passing through a low loss *elephant trunk* (Andrews LDF5-50A Heliax foam-filled) cable, and recorded by a fast digital scope which was set at a sampling rate of 1 GHz for a total of 512 (or sometimes 1024) channels for each turn. The bunch profiles were digitized every 25 to 75 turns. This sampling rate was sufficient to provide a detailed evolution of the beam profile in the diffusion process. A pretrigger to start data recording was set at least 100 ns prior to the arrival of the beam bunch.

Baseline measurements without applying phase modulation on either rf cavity were performed to calibrate the rf systems. The electron cooling system was optimized to attain a stable proton beam motion. The resulting bunch profile is

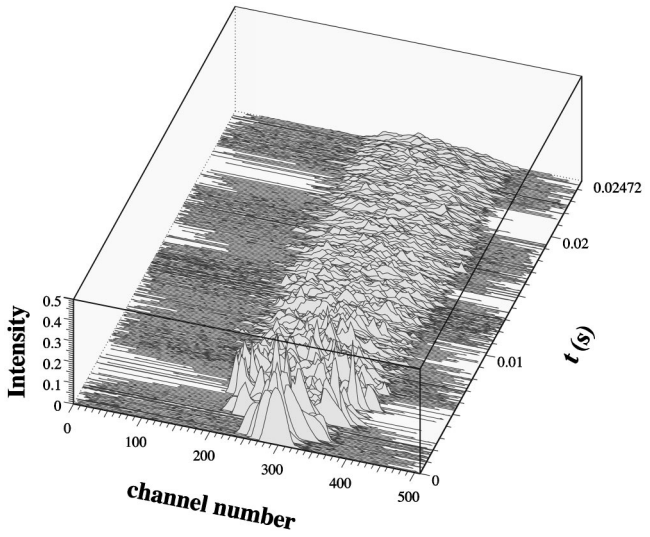


FIG. 1. A three-dimensional plot for the beam-profile evolution with phase modulation on the secondary rf system. The channel-number axis represents that a revolution time of about 969 ns was digitized into 512 channels, the time axis shows the resolution of 25 particle revolutions between two adjacent profiles, and the vertical axis depicts relative beam intensity. The modulation frequency $f_{m2}$ was set at 1400 Hz with modulation amplitude $A_2=100°$ and the rf voltage ratio $r=0.11$.

Gaussian-like with an rms beam width of $\sigma \approx 15$–$20$ ns, depending on the rf voltage and beam current. Since the solution of the Fokker-Planck-Vlasov equation of a stochastic dynamical system is given by Eq. (5), we can thus determine the diffusion coefficient of the beam particles in the Cooler with a known damping parameter.

The secondary rf system was turned on only when the data acquisition system began to take data. Two sets of experiments were carried out with phase modulation on the secondary and primary rf systems, respectively. Figure 1 shows a typical observed mountain-range plot of the evolution of the beam profile with an rf cavity voltage ratio $r=0.11$, where an rf phase modulation was applied only to the secondary rf cavity, with a modulation frequency $f_{m2}=1400$ Hz and a modulation amplitude $A_2=100°$. The three-dimensional plot shows the longitudinal beam distribution versus channel number in every 25 revolutions for the succeeding digitized profiles.

## IV. DATA ANALYSIS

The fast Fourier transform (FFT) spectra of the bunch centroid and the mean-square bunch length will be used to characterize experimental data. To understand the essential dynamics of the diffusion process, we perform extensive multiparticle simulations that include Gaussian white noise, electron cooling, and rf phase modulations in Eqs. (1) and (7). Comparing particle tracking simulations with the experimental data, we investigate the following physics phenomena: the bunch-shape evolution, the dynamics of the bunch dilution process, the role of parametric resonances in the diffusion process, and the physics of anomalous diffusion.

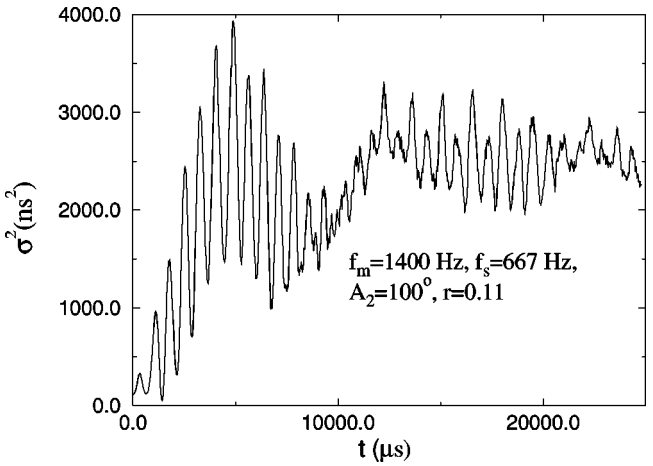


FIG. 2. Plots of $\sigma^2$ (ns$^2$) obtained from the experiment data shown in Fig. 1, for modulation frequency $f_{m2}=1400$ Hz, modulation amplitude $A_2=100°$, rf voltage ratio $r=0.11$, and harmonic number $h=9$.

### A. Evolution of bunch width in the presence of rf phase modulation

The evolution of the beam profile can be characterized by the motion of the centroid $\phi_{avg}$ and the mean-square (MS) bunch length $\sigma^2$. They are defined as

$$\phi_{avg}=\int \phi\rho(\phi)d\phi \approx \frac{1}{N}\sum_{i=1}^{N}\phi_i, \tag{11}$$

$$\sigma^2=\int (\phi-\phi_{avg})^2\rho(\phi)d\rho \approx \frac{1}{N}\sum_{i=1}^{N}(\phi_i-\phi_{avg})^2, \tag{12}$$

where $N$ is the number of particles in a beam bunch, $\phi_i$ is the phase coordinate of the $i$th particle, and $\rho(\phi)$ is the normalized density function. In our experiments, the bin size of the $\phi$ coordinate is 1 ns per channel.

A background subtraction is needed to analyze our data because of electronic noise. The averaged background level of our detection system can be calculated from the channels where there are no beam particles. The rms noise level $\sigma_{noise}$ was calculated from the first 40 channels. We then applied a $6\sigma_{noise}$ noise cut to our data to increase the signal-to-noise ratio. The noise cut is particularly important in the calculation of the mean-square bunch width and higher moments of the beam distribution.

Figure 2 shows a characteristic evolution of the mean-square bunch width, where the MS bunch length oscillates widely, and damps eventually into a constant that depends on parameters of the rf systems. On the other hand, Fig. 3 shows two examples of similar particle diffusion experiments at different modulation frequencies where the MS bunch lengths exhibit a smooth diffusion of linear or nonlinear growth and reach a saturation after about 10 ms. What causes the different behaviors of the particle diffusion mechanism? Can one identify the diffusion mechanism with the underlying stochasticity in the dynamical system? What role do the overlapping parametric resonances play in the diffusion process?

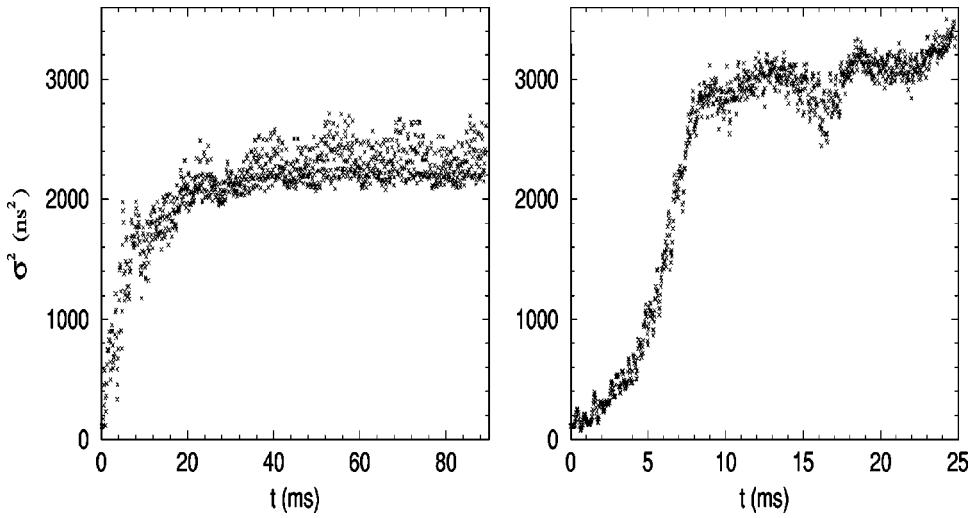


FIG. 3. Plots of $\sigma^2$ ($ns^2$) (derived from the measured data) for $A_2=50°$, $r=0.2$, and $f_{m2}=1100$ Hz (left) and 2700 Hz (right), respectively. The evolution of the MS bunch lengths differs from that of the top plot of Fig. 2. The left plot shows a characteristic linear growth of $\sigma^2$, while the right plot shows a characteristic anomalous diffusion.

### B. Phase modulation on the secondary rf cavity

In our experiment with a phase modulation applied to the secondary rf cavity, the rf phase-modulation amplitude, the modulation frequency, and the voltage ratio between the two rf cavities were systematically varied. Since the synchrotron frequency of our experiment was about 705 Hz, the modulation frequency was set to cover a range from 100 Hz to 3600 Hz with a 100 Hz step, and the modulation amplitude was set from about 10° to as high as about 400°. We tried to phase lock the primary and secondary rf systems in our experiments. However, we discovered during our data analysis that the relative phase of two rf systems was not properly locked when the control parameters were varied. The relative phase $\Delta\phi_0$ becomes a free parameter in fitting experimental data. Since the phase-space location of overlapping parametric resonances depends on the parameter $\Delta\phi_0$, the final phase-space distribution of the beam also depends on the relative phase parameter sensitively.

Figure 4 summarizes our data, where the final beam width is plotted as a function of the modulation frequency for the modulation amplitudes 65°, 100°, 125°, 150°, 175°, and 200°. Our results show that the beam response is particularly strong at modulation frequencies near the harmonics of the synchrotron frequency [11]. Our data analysis is therefore focused on the modulation frequencies about integer multiples of the synchrotron frequency.

#### *1. Effects of dominant parametric resonances in the chaotic sea*

In the following, we will show that the oscillatory structure of Fig. 2 for the first 10 ms arises from particles streaming along the separatrix of the dominant parametric resonances, and the decoherence of the coherent oscillation in $\sigma^2$ is due to the diffusion process into the chaotic sea [4]. Figure 5 shows $\sigma^2$ versus time for $\Delta\phi_0=245°$ and 180°, obtained from numerical simulations of 4000 particles in an initial Gaussian beam distribution, where we note that the resulting $\sigma^2$ depends sensitively on the relative phase $\Delta\phi_0$. The sensitivity on the relative rf phase can be understood as follows (see also Appendix A).

Neglecting the intrinsic diffusion term $D$ and phase-space damping term $\lambda$, the equations of motion can be cast into a Hamiltonian,

$$H=\frac{1}{2}\nu_s\delta^2+\nu_s\left[(1-\cos\phi)-\frac{r}{h}(1-\cos[h\phi+\Delta\phi_2])\right], \tag{13}$$

where $\Delta\phi_2$ is given in Eq. (9). The Hamiltonian can be divided into a time-independent term $\langle H\rangle$ and a time-dependent perturbation $H_1=H-\langle H\rangle$. Strong perturbation to particle motion occurs only when parametric resonances are excited by the time-dependent term [11]. The locations of the parametric resonances in the phase space are determined by the tune of the unperturbed Hamiltonian system. Since the ''equivalent time-averaged'' Hamiltonian of Eq. (13) depends sensitively on the parameter $\Delta\phi_0$, the final beam distribution also sensitively depends on the relative phase $\Delta\phi_0$.

The significance of the large amplitude oscillation in the MS beam width $\sigma^2$ observed in Fig. 2 can be understood easily by viewing the Poincaré surfaces of section of these

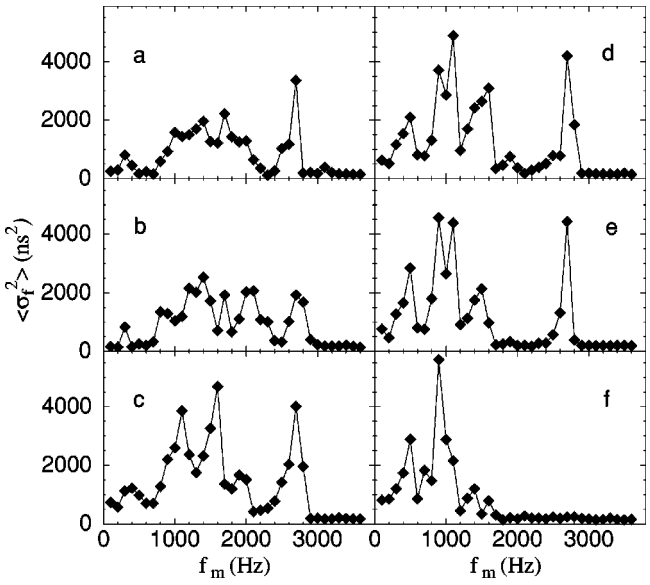


FIG. 4. Averaged final mean-square beam size $\langle\sigma_f^2\rangle$ versus modulation frequency for various modulation amplitudes. This is done by averaging the rms beam size over the last 5 ms of the data taken. The letters indicate the modulation amplitudes, where (a) is 65°, (b) is 100°, (c) is 125°, (d) is 150°, (e) is 175°, and (f) is 200°.

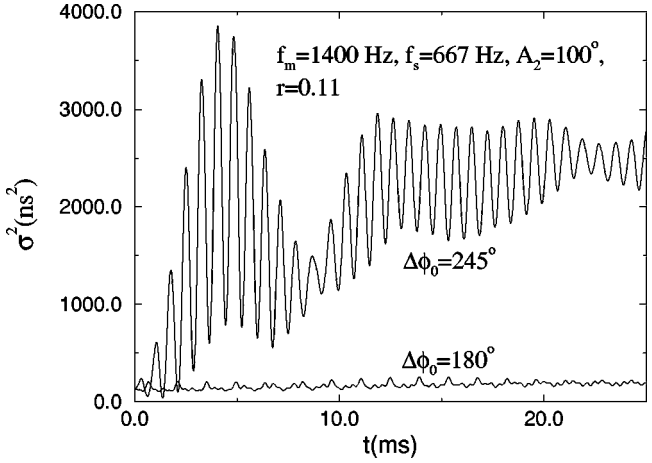


FIG. 5. Plots of $\sigma^2$ (ns$^2$) obtained from numerical simulations for two different values of the relative phase difference $\Delta\phi_0$, 180° and 245°, respectively, while keeping the other parameters the same. These calculations were carried out under the conditions $f_{m2}=1400$ Hz, $A_2=100°$, $r=0.11$, and $h=9$. The behavior of the beam depends sensitively on the value of the relative phase difference $\Delta\phi_0$.

two dynamical systems shown in the lower plots of Fig. 6. Since the initial phase-space area of the beam is small due to electron cooling, the final beam distribution depends on the actual chaotic region that overlaps with the initial phase space. The beam will evolve into a final distribution as shown in the upper plots bounded by invariant tori. Viewing the Poincaré surface of section, we find that the topology of the chaotic region depends sensitively on the parameters $\Delta\phi_0$ and $f_{m2}$.

Figure 7 shows the evolution of the phase-space distribution during the secondary rf phase modulation, where the

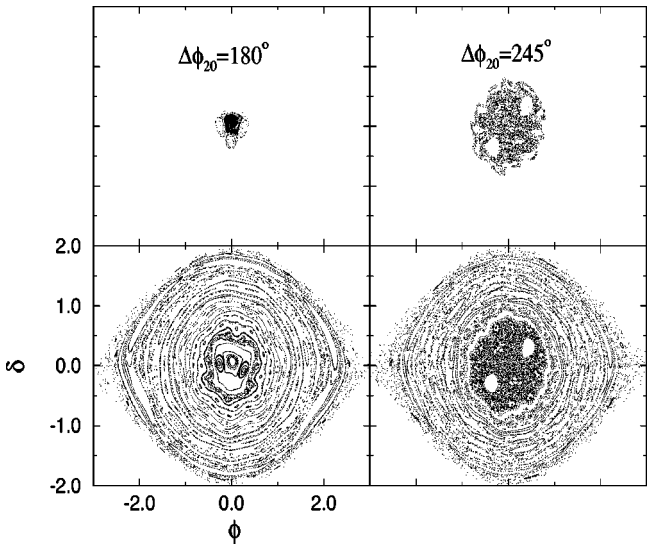


FIG. 6. Poincaré surfaces of section (bottom plots) and the final beam distribution obtained from numerical simulations (top plots) for two different values of the relative phase difference, $\Delta\phi_0=180°$ and 245°. These calculations were carried out under the same conditions as those of Fig. 5. Beam diffusion (or dilution) occurs only when the central region of the bucket becomes stochastic.

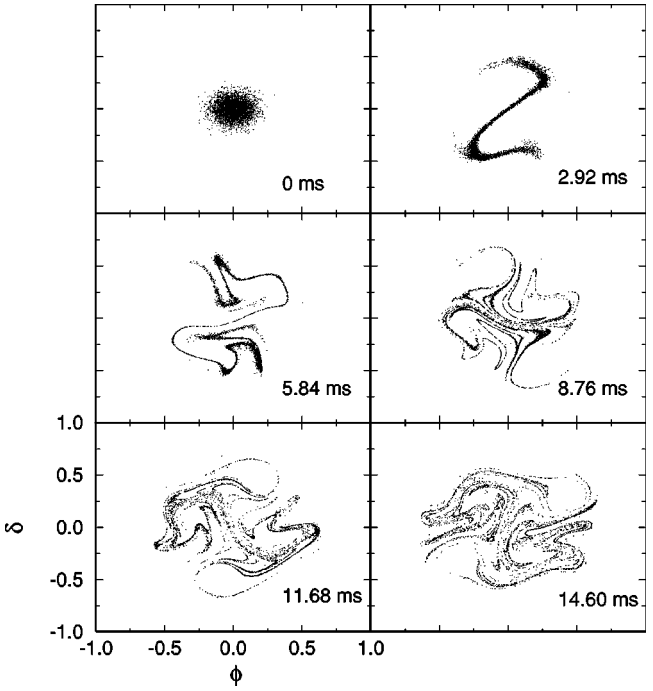


FIG. 7. Plots of the diffusion process for $f_{m2}=1400$ Hz, $A_2=100°$, $\Delta\phi_0=245°$, $r=0.11$, and $h=9$. Frame numbers are numbered in chronological order from 1 to 6 in time steps of 2.92 ms. The fast diffusion process is induced by two overlapping 2:1 parametric resonances.

first frame corresponds to the initial phase-space distribution and a time lapse of 2.92 ms in each succeeding frame. The large amplitude oscillation shown in Fig. 2 arises from the forced oscillation similar to that of the frame 2 in Fig. 7. The period of each oscillation shown in Fig. 5 corresponds to the period of the coherent synchrotron motion, i.e., two times the modulation period in this case. The maximum $\sigma^2$ corresponds to the time when particles diffuse into the maximum of the dominant parametric resonance. As particles gradually fill the chaotic sea of overlapping parametric resonances, the corresponding oscillatory amplitude in $\sigma^2$ will decrease and reach an equilibrium value. The final equilibrium phase-space areas of the beam shown in the upper plots of Fig. 6 are given by the phase-space areas of chaotic region.

The experimentally measured evolution of a beam distribution as a function of rf parameters in a storage ring reveals the particle diffusion mechanism along the separatrices of the dominant parametric resonances. A smooth uniform beam distribution requires not only a chaotic region in phase space formed by overlapping resonances, but also the chaotic sea bounded by invariant tori so that the beam distribution can be stabilized. The bunch evolution depends sensitively on rf parameters: the ratio of rf voltages $r$, the modulation frequency $f_{m2}$, the modulation amplitude $A_2$, and the relative phase $\Delta\phi_0$. We find that the evolution of the bunched beam can be divided into a fast process that is related to particle diffusion along the dominant parametric resonances and a slow process where particles diffuse inside the chaotic sea.

From our analysis, we find that a linear growth of $\sigma^2$ with time (see, e.g., the left plot of Fig. 3) can be identified as a diffusion process in a complete chaotic region in the phase

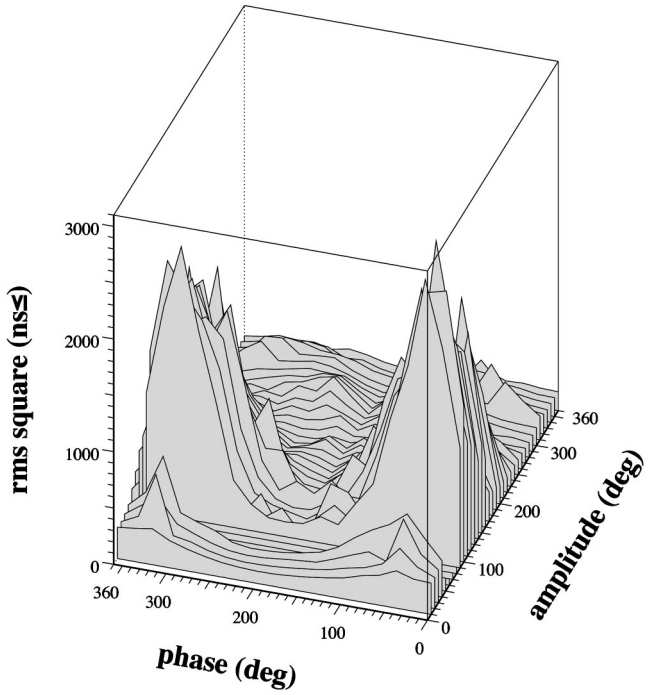


FIG. 8. The parameters used in tracking are the synchrotron frequency $f_{syn}=719$ Hz, $f_{m2}=1200$ Hz, and $r=0.11$. The final beam size is plotted as a function of the modulation amplitude $A_2$ (in degrees) and the relative phase $\Delta\phi_0$ (in degrees).

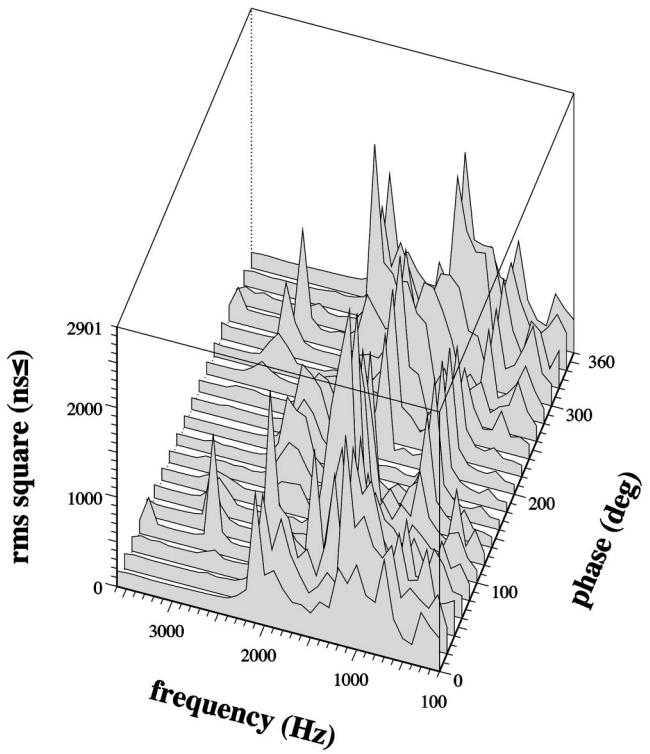


FIG. 9. The averaged equilibrium mean-square beam size is plotted as a function of modulation frequency $f_{m2}$ and modulation phase $\Delta\phi_0$. The parameters for the rf systems are $f_{syn}=720$ Hz with a modulation amplitude $A_2=100°$, rf voltage ratio $r=0.1$, and $h=9$.

space. On the other hand, if the phase space possesses a layer of chaotic sea with invariant tori embedded inside, then $\sigma^2$ will show characteristics of anomalous diffusion similar to the right plot of Fig. 3. However, if stable islands still exist in the chaotic background as shown in the lower right plot of Fig. 6, the evolution of $\sigma^2$ will be strongly oscillatory. Our experiment, with numerical simulations, has systematically verified these conditions. The understanding of the signature of the beam phase-space evolution can be used to diagnose the sources of emittance-dilution mechanisms in high brightness beams and space-charge dominated beams.

Because of the weak damping of the electron cooling system, the rf phase modulation by a secondary rf system can provide a chaotic dynamical system, where the attractors evolve into nonintersecting attracting curves, which depend sensitively on the value of the damping decrement λ and the intrinsic diffusion coefficient *D*. Such systems can also be detected by our beam measurement tools.

#### *2. Systematic numerical study of parametric dependence of particle diffusion*

Figure 8 shows the final mean-square beam width, obtained from numerical simulations of 4000 particles with Eqs. (1) and (7), as a function of the relative phase $\Delta\phi_0$ and a modulation amplitude $A_2$ with $f_{m2}=1200$ Hz and $f_{syn}=719$ Hz. Since the initial phase space area of the beam is small and the chaotic region moves with the relative phase $\Delta\phi_0$ and the amplitude $A_2$, the final beam width will peak at the relative phase and the modulation amplitude when the chaotic region overlaps with the initial phase-space area. The optimal modulation amplitude for the induced phase-space dilution occurs at a relative phase of 60° or 300° and the modulation amplitude of $A_2=100°-150°$, where the Bessel functions $J_1(A_2)$ and $J_2(A_2)$ are large (see Appendix A).

To determine the sensitivity of the phase-space dilution on the modulation frequency, we perform systematic tracking calculations using Eqs. (1) and (7) with rf parameters $r=0.1$, $A_2=100°$, and $f_{syn}=720$ Hz. Figure 9 shows the calculated $\sigma^2$ of the final beam distribution as a function of the modulation frequency $f_{m2}$ and the phase difference $\Delta\phi_0$. Note that the final beam width depends sensitively on the modulation frequency and the relative phase. The sharp peaks of strong beam excitation are located near the first, second, third, and fourth harmonic resonances.

#### *3. Dependence on the ratio of harmonic numbers*

The ratio of the harmonic numbers $h=h_2/h_1$ was chosen to be 9 in our experiments. To understand the dependence of the final beam emittance on the parameter *h*, we perform multiparticle numerical simulations for various harmonic ratio *h* with parameters $r=1/h$, $f_{syn}=720$ Hz, $f_m=1400$ Hz, and $A_2=100°$. Our results show that the entire bucket area can become chaotic for $h\leqslant 7$. When the entire bucket area becomes chaotic, the beam bunch will not be bounded by invariant tori, and particle loss becomes inevitable.

#### *4. Frequency spectra of experimental data*

Experimental data also show the sensitivity of the beam diffusion mechanism on the modulation frequency. Figure 10 shows the FFT spectra of the MS beam widths of all measured data with a modulation amplitude of 150°. A direct

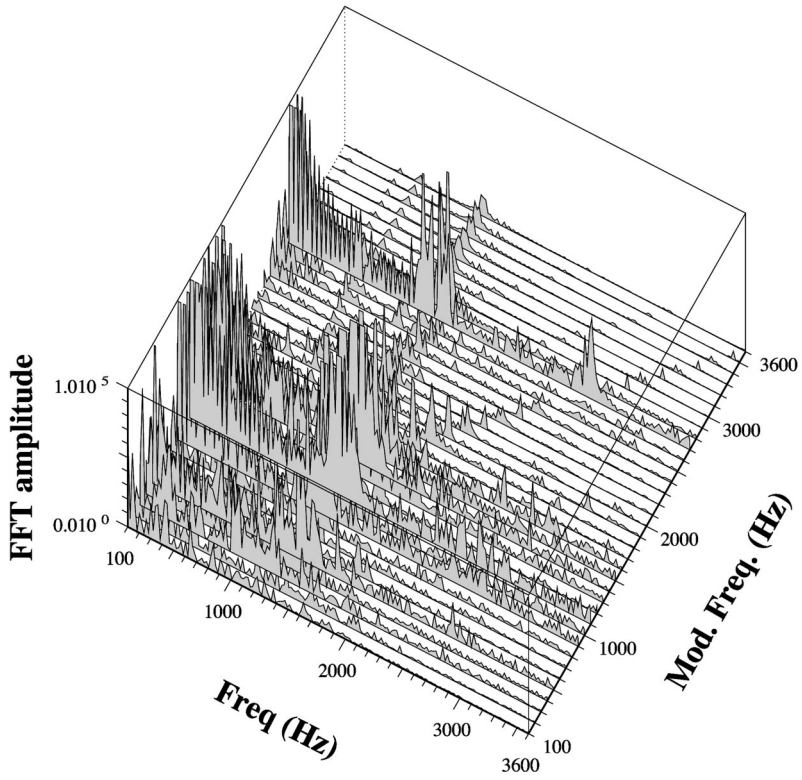


FIG. 10. The FFT spectra of the experimental data of mean-square beam widths for the modulation amplitude of 150°. We note that the low-frequency response in the data arises from the chaotic sea; the quadrupole and octupole modes arise from strong parametric resonances.

response line is visible in our data. Furthermore, the quadrupole and the octupole modes arising from the dominant parametric resonances are particularly strong when the modulation frequencies are driven at $2f_{\mathrm{syn}}$ and $4f_{\mathrm{syn}}$. We note also that when the beam is driven into a chaotic sea, the data show characteristic strong low-frequency response.

### C. Observation of the octupole mode

Our data show that the dominant excitation of synchrotron motion occurs between the first and third harmonics of the synchrotron frequency. However, we also note in Fig. 4 that a sharp peak appears near the modulation frequency of 2700 Hz, about four times the synchrotron frequency, in all modulation amplitudes except for $A_2 = 200°$ [12]. The experimental data shown in Fig. 4(b) indicate a substantial beam blow up at a modulation frequency of $f_{\mathrm{m2}} = 2700$ Hz.

To study the characteristics of the octupole mode, we performed multiparticle tracking calculations. Our numerical simulations shown in Fig. 9 indicate that the phases difference $\Delta\phi_0$ must be about 60° or 300°. Figure 11 shows the calculated Poincaré surface of section with various relative phase between the two rf systems, where the chaotic structure indeed arises from overlapping 4:1 parametric resonances.

Figure 12 shows the evolution of the beam bunch in the action of large octupolar excitation. Note that particles stream along the separatrices of the 4:1 parametric resonances before they diffuse into the chaotic sea. The large octupole response shown in Fig. 10 at the modulation frequency of 2700 Hz reflects this process. The low-frequency response arises from the process where particles diffuse gradually into the chaotic sea.

We have also performed many tracking calculations at modulation frequencies higher than 2700 Hz. We find that there is no significant beam dilution for modulation frequencies at or higher than 3600 Hz, which is about the fifth harmonic of the synchrotron frequency. Such results were also confirmed in our experimental measurements.

### D. Phase modulation on the primary rf cavity

Phase modulation on the primary rf system is much more sensitive to the beam than on the secondary rf system, be-

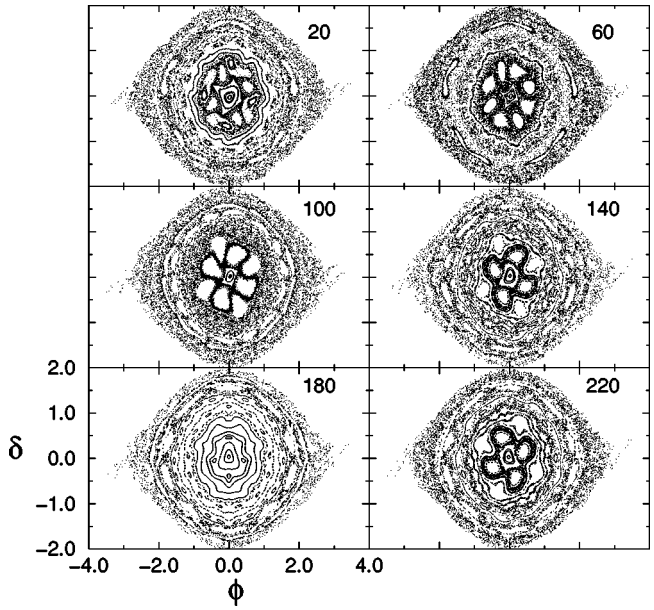


FIG. 11. The Poincaré surfaces of section for the modulation frequency of 2700 Hz with different relative phases. The rf parameters in the calculation are $A_2 = 100°$, $f_{\mathrm{m2}} = 2700$ Hz, $f_{\mathrm{syn}} = 685$ Hz, and $r = 0.1$. Note that the chaotic structure arises mainly from the overlapping resonances of 4:1 parametric resonances.

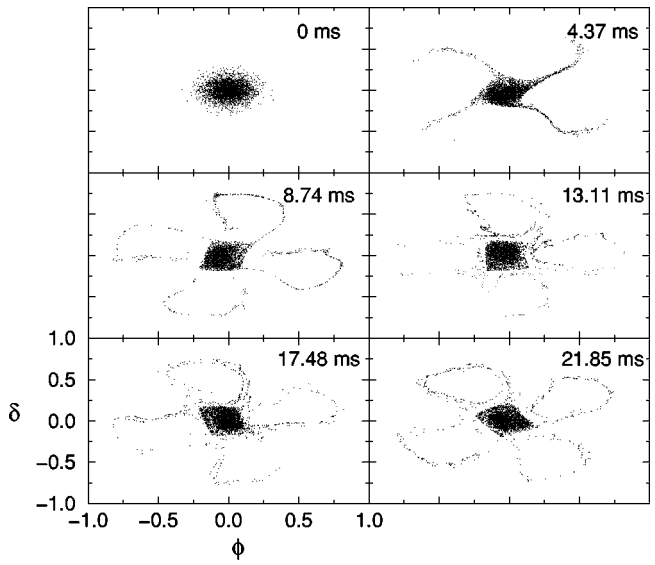


FIG. 12. The evolution of the bunch distribution showing the diffusion process that particles stream along the separatrices of the 4:1 parametric resonances. The rf parameters in the calculation are $A_2=100°$, $f_{m2}=2700$ Hz, $f_{syn}=685$ Hz, and $r=0.1$. They eventually diffuse into the chaotic sea. The octupole mode of excitation arises from these resonance structures.

cause the perturbation is much stronger [8]. Therefore, the modulation amplitude scan could not cover the entire $2\pi$ parametric space. The effect can be seen in the FFT spectra of the beam bunch centroid shown in Fig. 13. In this case, our data showed that particles were driven along the separatrix orbit and escaped the bucket at the unstable fixed point. Based on our experiments, it is advisable to modulate the secondary rf cavity for controlled bunch beam dilution.

## V. CONCLUSION

In conclusion, our experimental data show that the linear growth of $\sigma^2$ with time arises from the diffusion process in a complete chaotic region in the longitudinal phase-space. If the phase space exhibits a layer of chaotic sea with invariant tori embedded inside, $\sigma^2$ will show characteristics of anomalous diffusion. On the other hand, if stable islands remain in the chaotic background as shown in the lower right plot of Fig. 6, the evolution of $\sigma^2$ will be strongly oscillatory. Our experiment, and numerical simulations, have systematically verified these conditions. The understanding of the signature of the beam phase space evolution can be used to diagnose sources of emittance-dilution mechanisms in high brightness beams and space-charge dominated beams. The final phase-space area of the beam is determined essentially by the chaotic region in the phase space bounded by invariant tori.

We have experimentally measured the evolution of beam distribution as a function of rf parameters in a storage ring. These parameters are the ratio of rf voltages $r$, the modulation frequency $f_{m2}$, the modulation amplitude $A_2$, and the relative phase $\Delta\phi_0$. We have found that the evolution of the bunch beam can be divided into a fast process that is related to particle diffusion along the separatrices of dominant parametric resonances, and a slow process where particles diffuse inside a bounded chaotic sea.

We have also observed the octupole excitation. The corresponding phase-space evolution for the octupole excitation has been clearly measured. Particles stream through the separatrices of the 4:1 parametric resonance, and then diffuse into the chaotic sea. The signature of the beam signal can easily be identified.

## ACKNOWLEDGMENTS

The work was supported in part by grants from the U.S. DOE under Grant No. DOE-DE-FG02-92ER40747 and the NSF under Grant No. PHY-9512832.

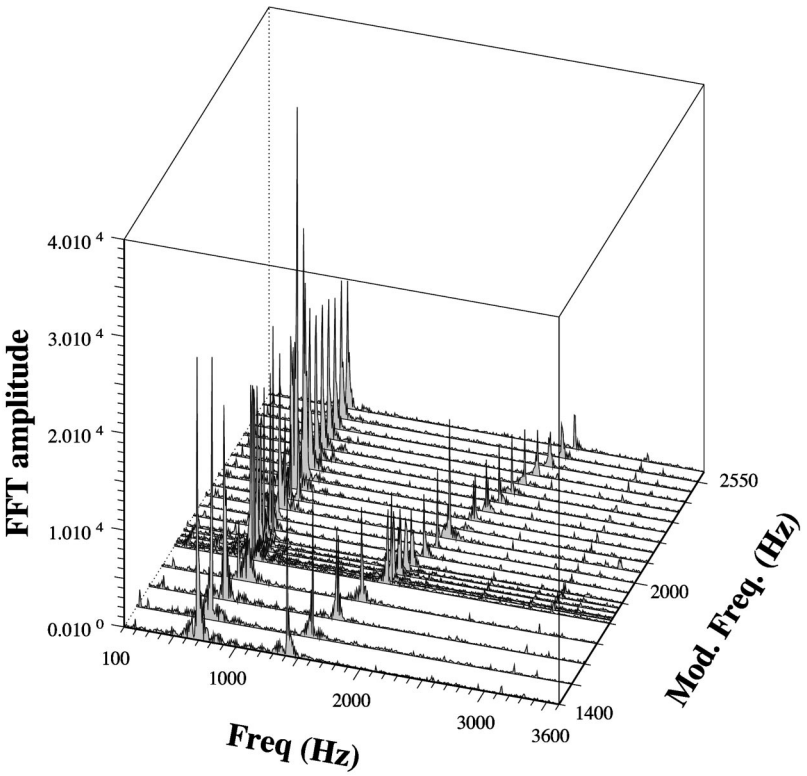


FIG. 13. An example of the FFT spectra for the averaged center position in the presence of the primary rf phase modulation. The modulation amplitude was about $A_1=4°$; the modulation frequency is applied from $f_{m1}=1400-2500$ Hz, with $h_2=9$, $r=0.1$. Note that the dipole mode is highly excited, and furthermore, the coherent driving oscillations, where the response frequency is equal to the driving frequency, are clearly visible.

## APPENDIX A: PROPERTIES OF THE TIME-DEPENDENT HAMILTONIAN

Without damping and the random noise terms, the Hamiltonian for synchrotron motion with an rf phase modulation to the secondary rf system is

$$H=\frac{1}{2}\nu_s\delta^2+\nu_s\left\{1-\cos(\phi)+\frac{r}{h}[1-\cos(h\phi+\Delta\phi_2)]\right\}$$
$$=\langle H(\delta,\phi)\rangle+\Delta H(\theta), \tag{A1}$$

where

$$\langle H\rangle=\frac{1}{2}\nu_s\delta^2+\nu_s\left\{1-\cos(\phi)+\frac{r}{h}[1-J_0(A_2)\cos(h\phi+\Delta\phi_0)]\right\}, \tag{A2}$$

$$\Delta H=-2\frac{\nu_s r}{h}\left[\cos(h\phi+\Delta\phi_0)\sum_{k=1}^{\infty}J_{2k}(A_2)\cos(2k\nu_{m2}\theta)-\sin(h\phi+\Delta\phi_0)\sum_{k=0}^{\infty}J_{2k+1}(A_2)\sin[(2k+1)\nu_{m2}\theta)]\right]. \tag{A3}$$

$J_k$ is the Bessel function of the order $k$. Since the time-averaged Hamiltonian $\langle H\rangle$ is $\theta$-independent, we will expand the Hamiltonian in the action-angle coordinates of $\langle H\rangle$. Defining the action coordinate as

$$J=\frac{1}{2\pi}\oint\delta(\phi)d\phi, \tag{A4}$$

we express $\langle H\rangle$ as a function of $J$, and obtain the synchrotron tune $Q_{\rm syn}=\partial\langle H\rangle/\partial J$ of an averaged double rf system, where $Q_{\rm syn}$ is a sensitive function of $\Delta\phi_0$ at small action $J$ [9].

Defining the generating function,

$$F_2(\phi,J)=\int_{-\hat{\phi}}^{\phi}\delta(\phi)d\phi, \tag{A5}$$

we obtain the conjugate phase coordinate as $\psi=\partial F_2/\partial J$. Now we can expand $\Delta H$ in action-angle coordinates of the time-averaged Hamiltonian as

$$\Delta H=\sum_{n,m}G_{n,m}(J)\cos(n\psi-m\nu_{\rm m}\theta+\chi_{n,m}), \tag{A6}$$

where $m$ and $n$ are integers, and $G_{n,m}$ and $\chi_{n,m}$ can be obtained from the Fourier expansion of $\Delta H$. When the modulation amplitude $A_2$ is not large, the perturbation depends essentially on two dominant terms, i.e., $\Delta H\approx G_{1,1}\cos(\psi-\nu_{\rm m}\theta+\chi_{1,1})+G_{1,2}\cos(\psi-2\nu_{\rm m}\theta+\chi_{1,2})$, where $G_{1,1}\propto J_1(A_2)$ and $G_{1,2}\propto J_2(A_2)$. Thus the effective perturbation will be peaked at a modulation amplitude $A_2\approx 100-150°$, where the values of $J_1$ and $J_2$ functions are maximum.

The perturbation $\Delta H$ of Eq. (A6) may contain many overlapping resonances where stationary phase conditions are encountered at a modulation tune $\nu_{\rm m}=n\dot{\psi}/m\approx nQ_{\rm syn}/m$. Overlapping resonances generate bounded chaotic regions in the phase space shown, for example, in Fig. 6.

### 1. Symmetry of the Poincaré surface of section

Since the Poincaré surface of section is obtained by plotting the phase-space point at $\nu_{\rm m}\theta=$ constant (mod $2\pi$), the Poincaré surfaces of section for dynamical systems with parameters $\Delta\phi_0$ and $2\pi-\Delta\phi_0$ are related by shifting $\nu_{\rm m}\theta\rightarrow\nu_{\rm m}\theta+\pi$ and $\phi\rightarrow-\phi$. Thus the effect of beam dilution for the rf systems with $\Delta\phi_0$ and $2\pi-\Delta\phi_0$ will be identical. For example, the Poincaré surfaces of section for $\Delta\phi_0=140°$ and 220° shown in Fig. 11 obey the symmetry condition. Similarly, the final mean-square bunch widths shown in Fig. 8 have similar symmetry property.

### 2. Effects of power supply ripple

In many beam manipulation experiments, it is very difficult to suppress the power supply ripple. The effect of the power supply ripple on the rf phase modulation can be represented by

$$\Delta\phi_2=[A_2+A_{\rm ripple}\sin(\nu_{\rm ripple}\theta+\chi_{\rm ripple})]\sin(\nu_{m2}\theta)+\Delta\phi_0$$
$$=A_2\sin(\nu_{m2}\theta)+\Delta\phi_0+\frac{1}{2}A_{\rm ripple}\sin[(\nu_{m2}-\nu_{\rm ripple})\theta-\chi_{\rm ripple}]-\frac{1}{2}A_{\rm ripple}\sin[(\nu_{m2}+\nu_{\rm ripple})\theta+\chi_{\rm ripple}]. \tag{A7}$$

Thus the power supply ripple produces modulation tunes $\nu_{m2}\pm\nu_{\rm ripple}$, and the beam spectrum will have 60 Hz sidebands around the dominant harmonics. This is evidently shown in the FFT spectra of experimental data in Figs. 10 and 13.

[1] V.V. Balandin, M.D. Dyachkov, and E.N. Shaposhnikova, Part. Accel. **35**, 1 (1991); R. Cappi, R. Garoby, and E.N. Shaposhnikova, Report No. CERN/PS 92-40 (RF) (1992); J.M. Kats, in *Proceedings of the 2nd European Particle Accelerator Conference* (Edition Frontières, Gif-sur-Yvette, France, 1990), p. 252; J.M. Kats, BNL AGS Technical Notes No. 324 (1989) (unpublished).

[2] High-intensity particle beams in synchrotrons can encounter transverse or longitudinal collective instabilities, particularly near the transition energy. Above the transition energy, a higher-energy particle takes a longer time to complete one revolution than that of the reference particle, as if it has a negative mass. Because all particles isochronously orbit around the synchrotron at the transition energy, i.e., the synchrotron tune becomes zero, the beam bunch can suffer a collective beam instability called the negative mass instability and

lead to uncontrolled beam loss. To minimize the effect of collective beam instability, one usually employs controlled beam manipulation schemes by reducing the line density of the circulating beam, or a faster acceleration rate. Similarly, at low energy, a double-rf system has been used to alleviate space-charge effects by reducing the peak current of the beam bunch. Since the double-rf system increases the synchrotron tune spread of the beam so that Landau damping is enhanced [9], and at the same time changes the time structure of the beam bunch so that the effective impedance is modified, it has also been used to overcome multibunch instabilities.

[3] R. Cappi, R. Garoby, and E.N. Shaposhnikova, Report No. CERN/PS 92-40 (RF) (1992); R. Cappi (private communications).

[4] D. Jeon *et al.*, Phys. Rev. Lett. **80**, 2314 (1998); K.Y. Ng, in *Proceedings of the Advanced ICFA Beam Dynamics Workshop on Beam Dynamics Issues for $e^+e^-$ Factories*, edited by L. Palumbo and L. Vignola, Frascat Physics Series Vol. X (Istituto Nazionale di Fisica Nucleare, Frascati, 1997), p. 227.

[5] M. Bai *et al.*, Phys. Rev. E **55**, 3493 (1997).

[6] See e.g., M.F. Shlesinger, G.M. Zaslavsky, and J. Klaften, Nature (London) **363**, 31 (1993), and references therein.

[7] See, e.g., C.L. Bohn and J.R. Delayen, Phys. Rev. E **50**, 1516 (1994); J. Struckmeier, *ibid.* **54**, 830 (1996), and references therein.

[8] M. Ellison *et al.*, Phys. Rev. Lett. **70**, 591 (1993); H. Huang *et al.*, Phys. Rev. E **48**, 4678 (1993); D. Li *et al.*, *ibid.* **48**, R1638 (1993); Nucl. Instrum. Methods Phys. Res. A **364**, 205 (1995).

[9] S.Y. Lee *et al.*, Phys. Rev. E **49**, 5717 (1994); J.Y. Liu *et al.*, *ibid.* **50**, R3349 (1994); Part. Accel. **49**, 221 (1995).

[10] R. Averill *et al.*, in *Proceedings of the 8th Conference on High Energy Accelerators*, edited by M.H. Blewett (CERN, Geneva, 1971), p. 301; P. Bramham *et al.*, IEEE Trans. Nucl. Sci. **NS-24**, 1490 (1977); J.M. Baillod *et al.*, *ibid.* **NS-30**, 3499 (1983); G. Gelato, L. Magnani, N. Rasmussen, K. Schindl, and H. Schroenauer, in *Proceedings of the IEEE Particle Accelerator Conference*, Washington, D.C. (IEEE, New York, 1987), p. 1298.

[11] See, e.g., S.Y. Lee, in *Accelerator Physics at the SSC*, edited by Y. Yan and M. Syphers, AIP Conf. Proc. No. 36 (AIP, New York, 1995), p. 13; S.Y. Lee, *Accelerator Physics* (World Scientific, Singapore, 1999).

[12] Small bunch dilution at $f_{m2}=2700$ Hz for $A_2=200°$ shown in Fig. 4(f) was probably due to an uncontrollable $\Delta\phi_0$ shift of the relative phase between two rf systems.